Surrogate models for predicting stall-induced vibrations on wind turbine blades

Santhanam, Chandramouli; Riva, Riccardo; Knudsen, Torben

Published in:
Journal of Physics: Conference Series (Online)

DOI (link to publication from Publisher):
10.1088/1742-6596/2265/3/032005

Publication date:
2022

Document Version
Publisher's PDF, also known as Version of record

Surrogate models for predicting stall-induced vibrations on wind turbine blades

Surrogate models for predicting stall-induced vibrations on wind turbine blades

Chandramouli Santhanam[1], Riccardo Riva[2], Torben Knudsen[1]

[1] Department of Electronic Systems, Aalborg University, Aalborg, Denmark
[2] Department of Wind Energy, Technical University of Denmark (DTU), Frederiksborgvej 399, 4000 Roskilde, Denmark

E-mail: chsa@es.aau.dk, ricriv@dtu.dk, tk@es.aau.dk

Abstract. Stall Induced Vibrations (SIV) are an aeroelastic instability that might happen when large portions of the wind turbine blade operate in moderate stall, which leads to high internal loads that can damage the structure. Exploring the inflow space that cause SIV has a high computational cost, which quickly increases with the number of input variables, since it involves high-fidelity aeroelastic simulations. In this work, a surrogate model is used to effectively explore the behavior of SIV in a five variable inflow space consisting of wind speed, yaw angle, vertical wind shear, wind veer, and atmospheric temperature. The surrogate model, trained from the results of a few aeroelastic simulations, predicts the severity of SIV for a given inflow condition. The surrogate model is chosen by comparing the performance of a few common model types, and Artificial Neural Networks (ANN) are found to provide a good balance between accuracy and computational time. Using the ANN, the occurrence and severity of SIV in the inflow space is studied. The analysis shows that for the turbine studied, yaw angle is the most influential variable, while temperature is the least influential variable in terms of conditions that lead to occurrence of SIV. Inflow conditions with a moderate yaw angle (around 10-25 deg), high wind speeds, and high negative veer are found to be the most critical in terms of severity of SIV. The current work is expected to serve as a helping tool to decide the focus of computationally expensive simulations such as high fidelity CFD based aeroelastic simulations.

1. Introduction

Stall Induced Vibrations (SIV) are an aeroelastic instability that might happen when large portions of the wind turbine blade operate in moderate stall (defined in this work as Angle of Attack (AoA) between 15 and 40 deg). This is typically due to a negative aerodynamic damping that happens as a result of the negative lift – AoA gradient [1]. Edgewise vibrations due to SIV were first observed and investigated in stall-regulated turbines [2, 3, 4]. Although modern pitch-regulated turbines do not operate in stall like the stall-regulated ones, computations still show that SIV can lead to extreme vibrations in the edgewise direction, in certain inflow conditions when the turbine is standing still [5]. These conditions are likely to happen when the turbines are parked for maintenance, during installation and after the cut-out wind speed, where the yaw angle can cause moderate stall. Apart from a risk of extreme loading to the blades, these vibrations also contribute to the fatigue loads on the blades, thereby reducing the lifetime of the blades. With the need to lower the Levelised Cost of Energy driving the design towards larger and more flexible wind turbine blades, SIV are an important design consideration.

SIV have been studied using the Blade Element Momentum theory (BEM) based solvers in the limited yaw angle range around moderate stall regions [6]. The Advanced Aerodynamic Tools for Large Rotors (AVATAR) project details a comprehensive comparative SIV study of BEM based aeroelastic solvers against a higher fidelity CFD based aeroelastic solver [7]. The results show that BEM-based solvers tend to over-predict standstill instabilities due to the utilization of static airfoil data. The study also identified the use of good quality airfoil data and the use of the right dynamic stall model to be key elements in predicting SIV using BEM-based engineering models. The validity of these engineering models decreases as we move into deep stall regions. Though the engineering models suffer such problems in predicting stall behaviour, they nonetheless offer a huge reduction in the computational cost, while still having respectable validity in moderate stall regions. The cost of an aeroelastic simulation to simulate 300 s is typically about 30 minutes, and it can be seen that the total computational cost increases drastically with the increasing number of dimensions to explore. Thus, even with the cost reduction offered by the engineering models, the exploration of the inflow space is still a very computationally expensive process.

As a solution to this problem, in this work, it is proposed to study the effect of inflow conditions on SIV using low cost alternatives to the simulations, namely surrogate models. Surrogate models establish a relationship between the inputs and outputs of the simulations that is quick to evaluate, and can be trained using the results of a few simulations. In the context of wind turbine design, surrogate models have been used for similar applications involving costly evaluations, such as evaluation of site specific loads [8], and study of the effect of multiple parameters on the blade design [9].

To the authors' best knowledge, the number of studies that have focused on the effect of inflow variables on SIV are very few, and the current work aims to add to this body of knowledge. The aim of this study is to explore the use of surrogate models to effectively explore the inflow space with respect to SIV i.e. understand the effect of inflow and environmental conditions on SIV. Studies of SIV in wind turbines [1, 10] show that the occurrence and severity of SIV depends on inflow conditions, airfoil characteristics and structural characteristics of the blade. With this motivation, the effect of five parameters are considered: wind speed, yaw angle, vertical wind shear, wind veer, and atmospheric temperature (which in turn affects the air density and the structural damping).

The outline of the paper is as follows. Section 2 explains the simulation setup and the inflow space. Evaluation of SIV stability and the generation of the database to train the surrogate model is discussed in section 3. Section 4 explains the choice of surrogate model. Section 5 discusses the effect of inflow conditions on the occurrence and severity of SIV. In section 6, some conclusions are drawn.

2. Simulation Setup and inflow space

In this work, the IEA 10MW turbine is chosen for investigation [11]. The occurrence and characteristics of SIV are studied for a parked rotor with 90 deg pitch angle, 0 deg azimuth angle (blade 1 pointing upwards), constant wind conditions, and only the blades are considered flexible. Hence only the individual blade modes are considered and not the turbine ones. The aeroservoelastic tool `HAWC2` [12] is used to obtain the response of the turbine for a given inflow condition. The aerodynamics, and the aeroelastic model of `HAWC2` has been verified against full CFD simulations and experiments in previous studies [13, 14]. The effect of dynamic stall is modelled through the MHH Beddoes dynamic stall method [1].

The inflow space consists of the five variables described in section 1. Parked conditions usually happen in a wind turbine when the wind speed is either below the cut-in speed or above the cut-out speed. However, wind speeds below the cut-in speed are not considered as they are too low to introduce substantial vibrations. This also justifies the consideration of 90 deg pitch

as the parking condition in this wind speed range is usually achieved by pitching the blades into the wind. For the considered pitch angle, it can be seen that negative yaw angles lead to stable conditions, while positive ones lead to SIV. Hence, only positive yaw angles are considered, and the yaw angle range is limited so as to avoid sections of the airfoil operating in deep stall where the engineering models have limited validity. The vertical wind shear exponent α is chosen to cover negative and positive shear. Wind veer is modelled through a coefficient a_φ as proposed in Ref. [15]

$$\Delta\varphi = \varphi(z) - \varphi(z_{hub}) \approx a_\varphi e^{-\sqrt{z_{hub}/h_{ME}}} \frac{z - z_{hub}}{\sqrt{z_{hub} h_{ME}}} \left(1 - \frac{z - z_{hub}}{2\sqrt{z_{hub} h_{ME}}} - \frac{z - z_{hub}}{4 z_{hub}}\right), \quad (1)$$

where z represents the height of the point, $\Delta\varphi(z)$ represents the veer angle at height z, z_{hub} is the hub height, h_{ME} is the modified Ekman atmospheric boundary layer depth here set to 500 m. The constant a_φ depends on wind parameters and can be considered site-specific, and a recommended range given in [15] is [-1.2, 0.5]. As it can be seen from Eq. (1), positive values of a_φ correspond to positive veer angles above the hub and negative veer angles below the hub (veering), while negative values of a_φ correspond to negative veer angles above the hub and positive veer angles below the hub (backing). Also, $a_\varphi = 0$ corresponds to zero veer, and values further from zero imply higher veer in the respective direction. Practically, a_φ is a scaling factor to represent the veer. The ranges of the considered variables are shown in table 1.

Table 1: Ranges of the considered variables

Variable	**Range**
Wind speed	[25, 60] ms^{-1}
Yaw Angle	[0, 40] deg
α	[-0.1, 0.4]
a_φ	[-1.2, 0.5]
Temperature	[-15, 20]°C

The effect of temperature is that it leads to a change in air density and structural damping of the blade modes. The relation between temperature and air density is modelled using the ideal gas equation. The structural damping of glass fiber composite materials similar to the ones used in wind turbine blades increases with the temperature [16]. However, the exact nature of the variation depends on the fiber material used in the blades, and the fiber orientation. In this work, a linear variation between temperature and structural damping is assumed. The reference temperature for the normal damping values is considered as 15 °C, and a decrease of 50% in the structural damping is assumed at −10 °C. The variation of the damping of the first three modes with temperature is shown in Fig. 1.

In `HAWC2`, structural damping is modelled using the Rayleigh damping model where the damping matrix is written as $C = \alpha M + \beta K$ where M and K are the mass and stiffness matrices respectively, and $\alpha = [\alpha_x \quad \alpha_y \quad \alpha_z]$ and $\beta = [\beta_x \quad \beta_y \quad \beta_z]$ are coefficients. Typically, while creating `HAWC2` models α is set to zero, and the values of β are tuned until the required structural damping is achieved. For a given value of α and β, and the structural model of the turbine blade, the structural damping can be quickly calculated using the program `HAWC2S` [17]. To calculate the value of β for a given temperature, the new values of damping of the first three modes are first calculated, and the values of β_x, β_y, β_z are tuned using `HAWC2S` until the new damping values for the first three modes are achieved. The tuning is framed as an optimization problem with a cost function $C = \sum_{i=1}^{3} (\zeta_i - \zeta_{i,req})^2$, where ζ_i represents the damping of the i^{th}

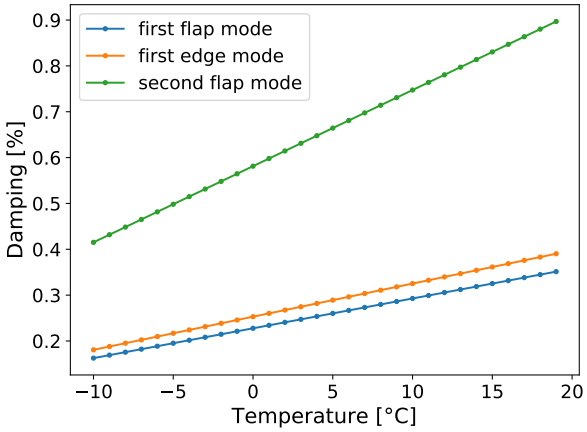

Figure 1: Variation of damping of the first three blade modes with temperature

mode for a given β, and $\zeta_{i,req}$ represents the required damping for a given temperature. The optimization problem is solved using `OpenMDAO` [18].

3. SIV Stability and database

3.1. Stability Characterisation

The edgewise bending moment at the root of blade 1 is chosen as the response to characterise SIV. Thus, a growth of edgewise bending moment with time implies the presence of SIV while a decay implies the absence of SIV. The behaviour of the wind turbine for different inflow conditions broadly falls into three categories: linearly stable, linearly unstable and non-linearly unstable (where the system enters a limit cycle after some time). The corresponding edgewise bending moments are shown in Fig. 2.

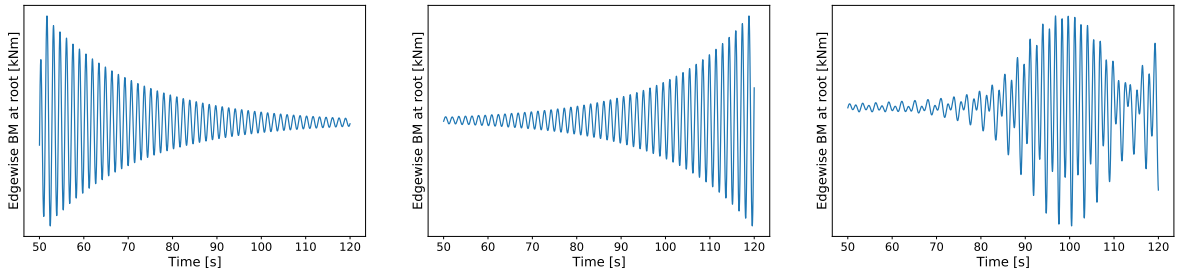

(a) *Linearly Stable.* **(b)** *Linearly Unstable.* **(c)** *Nonlinearly Unstable.*

Figure 2: Stable and Unstable responses

The severity of SIV is estimated by identifying the damping ratio of the first blade edgewise mode . The first 50 s is discarded as transient. The response is then limited in time to be in the linear range to make it suitable for a damping identification method. Different methods were attempted to identify the damping ratio - fitting an Auto Regressive (AR) model to the time series, the classical logarithmic decrement method, and a variant of the logarithmic decrement based on computing the slope of the straight line passing through the logarithm of the response peaks. While the AR model can identify multimodal responses, it faces difficulties with noisy responses. The logarithmic decrement method is very dependent on the choice of peaks, and different peaks in the same response can lead to identification of significantly different damping

ratios. The variant of the logarithmic decrement method avoids this problem by considering many peaks, and hence is more robust. Of these methods, the variant of the log decrement method is eventually chosen for its robustness. The damping ratio is identified using this method as follows: Let ω_d represent the damped frequency of the dominant blade mode, which in the case of SIV is the first edgewise mode. ω_d can thus be identified as the frequency corresponding to the peak of the power spectral density of the response. The response, band-pass filtered around ω_d can be written as

$$y(t) = Ae^{-\zeta\omega_n t}\sin(\omega_d t + \phi), \tag{2}$$

where ζ represents the mode damping ratio, and ω_n the mode natural frequency, which is related to ω_d as $\omega_d = \omega_n\sqrt{1-\zeta^2}$. It can be seen that for low values of ζ, $\omega_n \approx \omega_d$. This approximation is valid in the context of SIV, which are not expected to have very high values of ζ. In eq. (2), the term $Ae^{-\zeta\omega_n t}$ indicates the growth/decay of the peaks of the response , and so by indicating with (t_i, p_i) the time and value of the i^{th} response peak, it can be written that

$$\log(p_i) = -\zeta\omega_n t_i + c, \tag{3}$$

where c is the line intercept. Thus, the mode damping ratio can be calculated from the slope of the straight line fitted to the logarithm of the bandpass filtered response peaks and the corresponding time instances. The straight line is fit with the least-squares method.

3.2. Database generation and surrogate model training

The database necessary to train surrogate models is generated with 1000 points in the inflow space and the corresponding damping ratios identified from the results of the `HAWC2` simulations. To be able to build useful surrogate models that can predict the behaviour of SIV in the inflow space, it is important to ensure that the database has enough points with a negative damping (presence of SIV). To ensure this, the following method is used to generate the samples. Roughly, the following conditions are guessed as being favourable for SIV - high wind speeds, moderate yaw angles, and low temperatures. So a trapezoidal distribution is considered for wind speed, yaw, and temperature with a high density at high wind speeds, moderate yaw angles, and low temperatures respectively. The effect of α and a_φ are not guessed beforehand, and hence a uniform distribution is considered for α and a_φ. The samples for the database are generated using a Latin Hypercube Sampling (LHS) method to avoid generation of correlated samples and avoid generation of clustered samples in the multidimensional space. The marginal PDFs and the pair plots of the samples are shown in figure 3. The library `OpenTURNS` [19] is used to generate the samples using LHS Design.

Surrogate models that establish an input output relation between the inflow variables and the corresponding damping ratio are then trained on this database. The surrogate models considered are: Artificial Neural Network (ANN), Linear Interpolation, a Radial Basis Function (RBF), and a Gaussian Process Regression (GPR) with a Matern Kernel. The linear interpolation, RBF, and GPR models are considered because they predict the exact value at the training points. Given that the output of a simulation is computationally expensive, this feature of the models makes them an attractive choice. ANN is considered because it has the ability to fit highly nonlinear functions, which is expected to be a characteristic of the damping ratio in the considered inflow space.

The input and output variables are normalized to the range [0, 1], and the surrogate models are trained on the normalized data. And similarly, whenever a prediction is to be made using the trained model, the data is normalized to [0, 1] and the resulting output is then inverse scaled to obtain the predicted damping ratio. For the ANN, RBF, and GPR models, 60% of the samples are used for training, 20% for validation, and 20% are used for testing. Since the linear interpolation model does not have any hyperparameters to be tuned using the validation

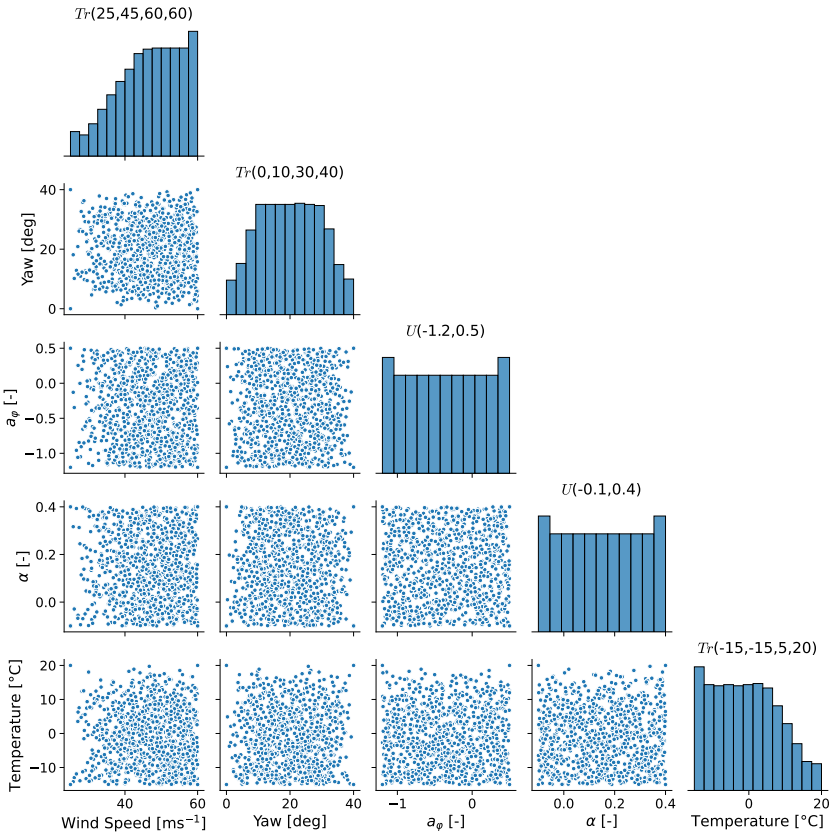

Figure 3: Marginal PDFs of the variables and the samples. Tr represents a trapezoidal distribution and U represents a uniform distribution

data, 80% of the data is used for training, and 20% is used for testing. The model accuracy is measured using the coefficient of determination, R^2 calculated on the test data set.

4. Performance of Surrogate models

Since a large number of evaluations are required to analyse the behaviour of SIV in the inflow space, the prediction speed of the surrogate models is of great relevance. Additionally, the models must also have an accuracy as high as possible. The right surrogate model is hence chosen based on these criteria. The models are ranked based on their accuracy and prediction speed, as shown in figure 4. Of the surrogate models investigated, ANN is found to provide a good balance between accuracy and prediction speed. The ANN is constructed using the `TensorFlow` library [20]. It has an input layer with 8 neurons, and two hidden layers with 6 neurons each. It is to be noted that with respect to the time taken to train the models, ANN has a high training time while the other models require significantly less time for training. But the choice of ANN is justified since the training time is a one time cost as compared to the surrogate evaluations which may be needed many times for analysis.

5. Influence of inflow conditions on SIV

5.1. Effect of inflow conditions on occurrence

In a multi dimensional domain, the effect of a particular variable on the output is not readily seen, as it may depend on the values of the other variables. In such a setting, large number of evaluations are necessary to analyse the effect of the variables on the output, and also analyse

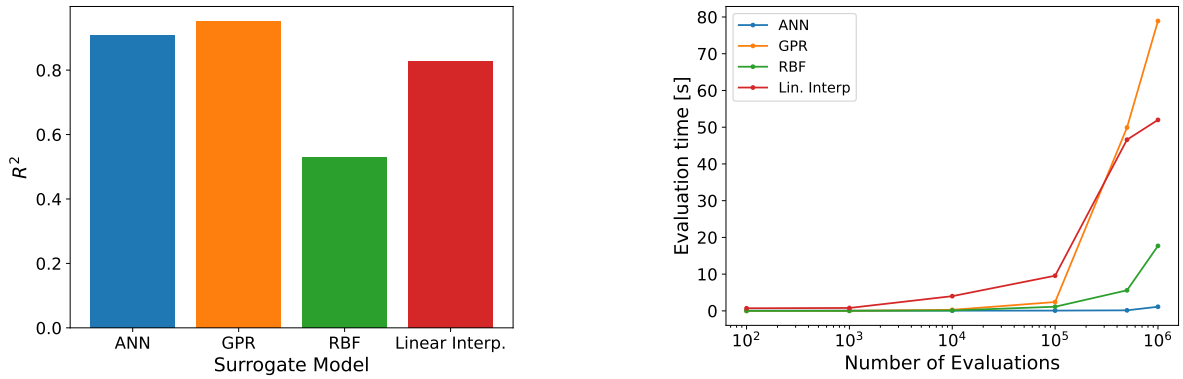

(a) R^2 *of the models calculated on the test dataset.* **(b)** *Prediction speed of the different models.*

Figure 4: Accuracy and prediction speed of the surrogate models

the effect of interaction between the variables as different combinations may affect the output differently. In these scenarios, surrogate models are a very useful tool as they can quickly make a large number of evaluations. The behaviour of SIV in the considered inflow space is analysed using methods inspired from Regional Sensitivity Analysis. We denote an inflow space variable as X_i, where $i = \{1, 2, 3, 4, 5\}$ denotes the index of each variable. For each X_i, n_i equally spaced levels are defined, and a 5-dimensional rectangular grid is constructed. Using the ANN, a prediction of the damping ratio (ζ) is made over the grid. Then, for each X_i, the probability of occurrence of SIV at a particular level ($X_i = x_i^{(j)}$) is calculated as the ratio of number of conditions (n) in which SIV are observed to the total number of conditions at that level.

$$P_{SIV}(X_i = x_i^{(j)}) = \frac{n(X_i = x_i^{(j)}; \zeta < 0)}{n(X_i = x_i^{(j)})}. \tag{4}$$

This quantity is proposed as a measure of the importance or influence of individual variables in the multidimensional inflow space. A flat variation of $P_{SIV}(X_i)$ with X_i indicates that all values of X_i can lead to instability, and hence the influence of X_i is not strong. On the other hand, a steep variation indicates that certain values of X_i lead to instability more than other values, and hence the influence of X_i is strong. The variation of P_{SIV} with all the inflow variables is shown in Fig. 5.

It can be seen that yaw angle is the most influential variable with high probability of occurrence of SIV at higher values of yaw while shear and temperature are the least influential variables, as the probability of occurrence is nearly constant across all values of these variables. Wind speed and wind veer seem to have a mild influence on the occurrence of SIV.

The longer the portion of the blades experiencing stall, the more severe is the SIV. This explains the increase of incidence of SIV with increasing yaw angle. As the yaw angle increases, the sections of the blade start experiencing stall, with the stalled portion of the blade increasing with increasing yaw angle. Similarly, as the negative veer increases, the outboard portions experience stall, which increases SIV. The reason for the very low influence of temperature is that the effect of temperature is modelled through a change in structural damping, and for the turbine considered, the structural damping of the first edgewise mode is low (0.36%) as compared to the negative aerodynamic damping, which can be as high as −5%. Therefore, changes in temperature do not affect the overall damping significantly.

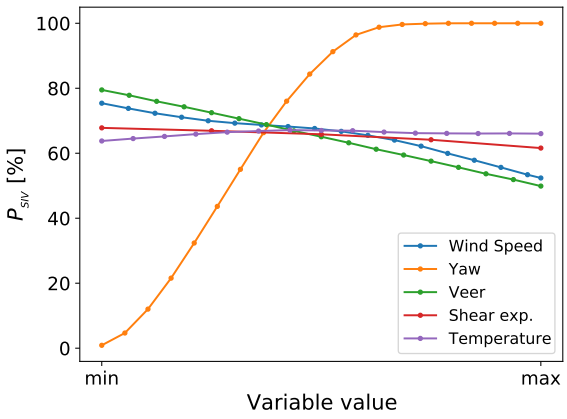

Figure 5: Predicted probability of occurrence of SIV for each variable

To understand the influence of the interaction of variables, a similar analysis is done, by considering the joint probability of occurrence of SIV for different combinations of the levels of variables (similar to a bi-variate histogram). Let i and j denote the indices of the variables with k_i and k_j levels respectively. Then the joint probability of occurrence of SIV for the combination m_1^{th} level of X_i & m_2^{th} level of X_j is defined as

$$P^*_{SIV}(X_i = x_i^{(m_1)}; X_j = x_j^{(m_2)}) = \frac{n(X_i = x_i^{(m_1)}; X_j = x_j^{(m_2)}; \zeta < 0)}{n(X_i = x_i^{(m_1)}; X_j = x_j^{(m_2)})}. \tag{5}$$

To understand the interaction among the variables, the combinations with respect to yaw angle are the most beneficial to analyse since yaw is the most influential variable. The contour plots of the joint probability of occurrence of SIV for combinations of yaw angle with the other variables is shown in Fig. 6.

From Fig. 6a, it can be seen that conditions with a negative veer are more critical than those with positive veer. With a moderate to high negative veer coefficient, SIV can happen even at very low yaw angles, while with a positive veer, the threshold of yaw angle at which SIV is expected to occur is much higher. With respect to wind speed, it can be seen from Fig. 6b that the yaw angle threshold for SIV stability is higher at higher wind speeds. In Fig. 6c and 6d, the combinations with yaw angle and shear and yaw angle and temperature show a variation predominantly in the yaw direction, indicating that shear and temperature do not have a significant impact on deciding the threshold for the yaw angle at which SIV are likely to occur.

5.2. Effect of inflow conditions on severity

To assess the most severe conditions with respect to SIV, the damping ratio at different inflow conditions is analysed. Since yaw angle is the most decisive variable, followed by a_φ and wind speed with a mild influence, the variation of damping ratio with yaw and a_φ, and yaw and wind speed as predicted by the surrogate model is analysed. Temperature and shear exponent are fixed at the following values: temperature = 15 °C, $\alpha = 0.1$.

Since the influences of wind speed and a_φ are not known, the variation of damping ratio and a_φ is analysed for two different values of wind speed, close to the extremes at 30 ms^{-1} and 55 ms^{-1} . Similarly, the variation of damping ratio and wind speed is analysed for different values of a_φ at -0.9 and 0.2. The variations are shown in figures 7 and 8.

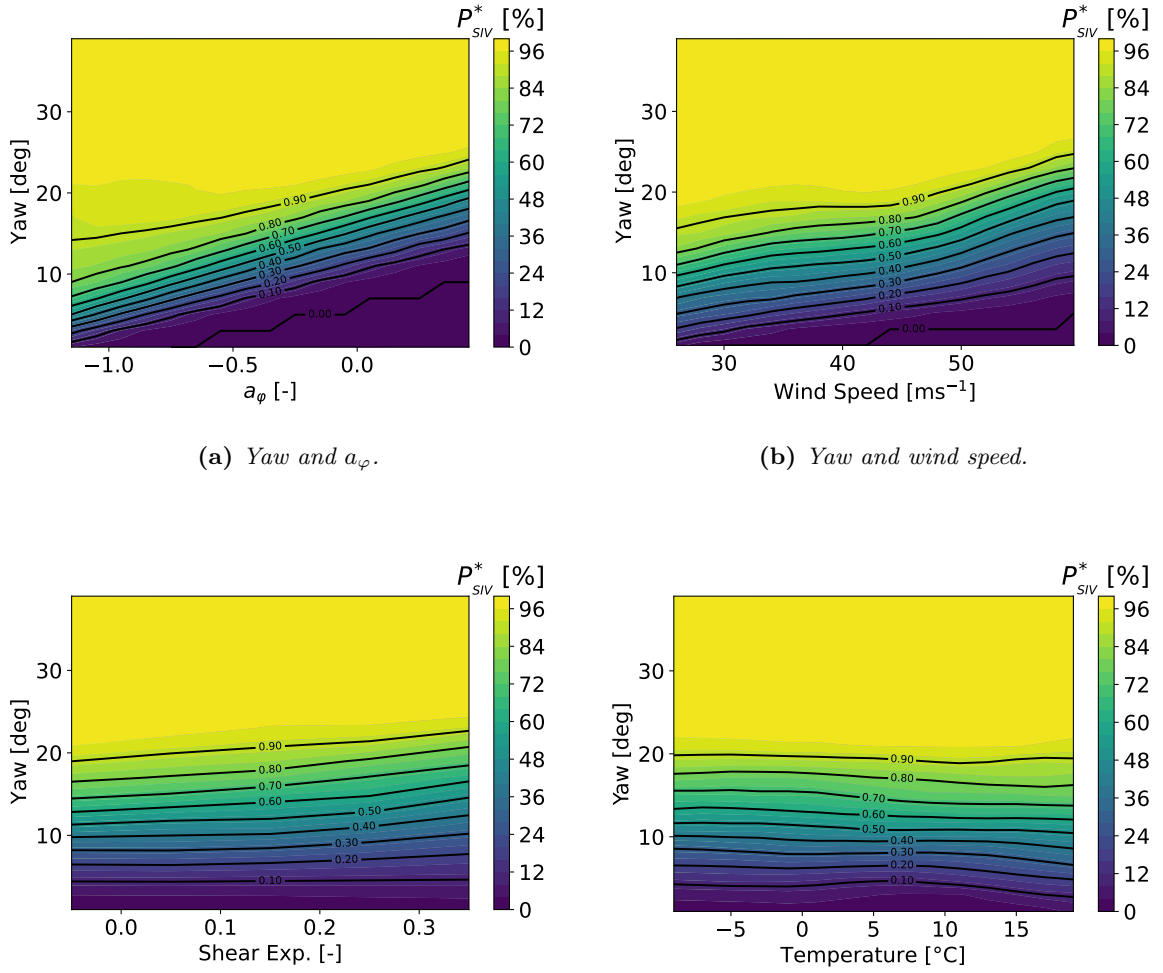

(a) *Yaw and* a_φ.

(b) *Yaw and wind speed.*

(c) *Yaw and shear.*

(d) *Yaw and temperature.*

Figure 6: Predicted joint probability of occurrence of SIV for combinations of variables.

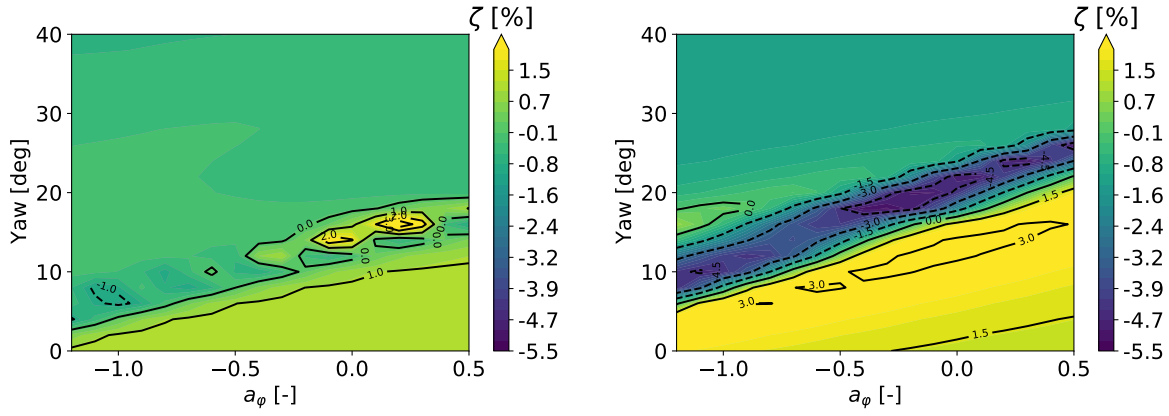

(a) *Wind speed* $= 30ms^{-1}$

(b) *Wind speed* $= 55ms^{-1}$

Figure 7: Variation of damping ratio with yaw and a_φ

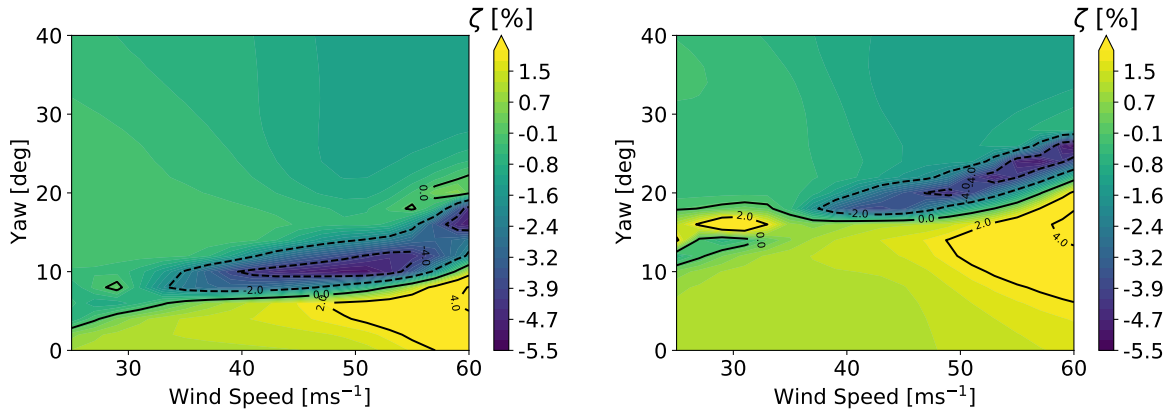

(a) $a_\varphi = -0.9$ **(b)** $a_\varphi = 0.2$

Figure 8: Variation of damping ratio with yaw and wind speed

It can be seen that yaw angles from 10 to 25 deg are the most critical. In this region, the transition from a stable response to an unstable response occurs. The critical conditions happen at low yaw angles at high negative veer, and at a higher yaw angle at positive veer. Since the occurrence of SIV is not affected very much by a particular choice of value for temperature and shear, the conclusions drawn above are expected to hold across the whole range of temperature and shear in the inflow space.

It is to be noted that the severity of SIV as described in this work is measured using the damping ratio at low amplitude levels. However, the simulations are performed using a BEM-based aeroelastic solver, and as mentioned earlier, these solvers tend to over-predict the instabilities. Hence a more accurate picture of SIV are expected using the high cost, high fidelity CFD based aeroelastic solvers. But the methods presented in this study are expected to serve as useful tools to narrow the inflow conditions to be simulated using the CFD solvers, thereby optimizing the computational cost required to explore the inflow space.

6. Conclusions

In this work, the use of a surrogate model such as an Artificial Neural Network to understand the behaviour of SIV in a given inflow space is demonstrated. Using the trained surrogate model, a quick estimate of the turbine stability for any given inflow condition can be obtained instead of performing a computationally expensive aeroelastic simulation. Further, the usefulness of the surrogate model to study the sensitivity of SIV with respect to the inflow variables, and to assess the inflow conditions that lead to severe SIV is demonstrated.

The following works are planned as an extension and as topics of a future publication:

- Develop a framework to optimally select samples in a n-dimensional inflow space for training the surrogate models
- Develop a similar methodology to study other flow induced vibrations, such as Vortex Induced Vibrations.

Acknowledgments

This research has been supported by Innovation Fund Denmark (grant no. 9090-00025B).

References

[1] Morten H Hansen. Aeroelastic instability problems for wind turbines. *Wind Energy: An International Journal for Progress and Applications in Wind Power Conversion Technology*, 10(6):551–577, 2007.

[2] Morten H Hansen. Improved modal dynamics of wind turbines to avoid stall-induced vibrations. *Wind Energy: An International Journal for Progress and Applications in Wind Power Conversion Technology*, 6(2):179–195, 2003.

[3] K Thomsen, J T Petersen, E Nim, S Øye, and B Petersen. A method for determination of damping for edgewise blade vibrations. *Wind Energy: An International Journal for Progress and Applications in Wind Power Conversion Technology*, 3(4):233–246, 2000.

[4] J T Petersen, Helge A Madsen, Anders Björck, Peder Enevoldsen, Stig Øye, Hans Ganander, and Danny Winkelaar. Prediction of dynamic loads and induced vibrations in stall. Technical report, RISO-R-1045(EN), 1998.

[5] Witold Skrzypiński and Mac Gaunaa. Wind turbine blade vibration at standstill conditions-the effect of imposing lag on the aerodynamic response of an elastically mounted airfoil. *Wind Energy*, 18(3):515–527, 2014.

[6] E S Politis, P K Chaviaropoulos, V A Riziotis, S G Voutsinas, and Ignacio Romero-Sanz. Stability analysis of parked wind turbine blades. In *Proceedings of the EWEC*, pages 16–19. Scientific Track, Marseille, 2009.

[7] Joachim C Heinz, Niels N Sørensen, Vasilis Riziotis, Michael Schwarz, Sugoi G Iradi, and Michael Stettner. Aerodynamics of large rotors. WP4. deliverable 4.5. *AdVanced Aerodynamic Tools for lArge Rotors (AVATAR)*, 2016.

[8] Nikolay Dimitrov, Mark C Kelly, Andrea Vignaroli, and Jacob Berg. From wind to loads: wind turbine site-specific load estimation with surrogate models trained on high-fidelity load databases. *Wind Energy Science*, 3(2):767–790, 2018.

[9] Thanasis Barlas, Néstor R García, Georg R Pirrung, and Sergio G Horcas. Surrogate-based aeroelastic design optimization of tip extensions on a modern 10MW wind turbine. *Wind Energy Science*, 6(2):491–504, 2021.

[10] M Stettner, M J Reijerkerk, A Lünenschloß, V Riziotis, Alessandro Croce, Luca Sartori, Riccardo Riva, and J M Peeringa. Stall-induced vibrations of the AVATAR rotor blade. In *Journal of Physics: Conference Series*, volume 753, page 042019. IOP Publishing, 2016.

[11] Pietro Bortolotti et al. IEA wind task 37 on systems engineering in wind energy WP2.1, reference wind turbines. Technical report, International Energy Agency, 2019.

[12] Torben J Larsen et al. How 2 hawc2, the user's manual. Technical report, DTU Wind Energy, Risø-R-1597, 2007.

[13] Torben J Larsen, Helge A Madsen, Gunner C Larsen, and Kurt S Hansen. Validation of the dynamic wake meander model for loads and power production in the egmond aan zee wind farm. *Wind Energy*, 16(4):605–624, 2012.

[14] Helge A Madsen, Torben J Larsen, Georg R Pirrung, Ang Li, and Frederik Zahle. Implementation of the blade element momentum model on a polar grid and its aeroelastic load impact. *Wind Energy Science*, 5(1):1–27, 2020.

[15] Anand Natarajan et al. Demonstration of a basis for Tall Wind Turbine Design, EUDP project final report. Technical report, DTU Wind Energy E, No. 0108, 2016.

[16] Youssef Sefrani and Jean-Marie Berthelot. Temperature effect on the damping properties of unidirectional glass fibre composites. *Composites Part B: Engineering*, 37(4-5):346–355, 2006.

[17] Morten Hansen. Aeroelastic properties of backward swept blades. In *49th AIAA Aerospace Sciences Meeting Including the New Horizons Forum and Aerospace Exposition*, page 260, 2011.

[18] Justin S. Gray, John T. Hwang, Joaquim R. R. A. Martins, Kenneth T. Moore, and Bret A. Naylor. OpenMDAO: An open-source framework for multidisciplinary design, analysis, and optimization. *Structural and Multidisciplinary Optimization*, 59(4):1075–1104, April 2019.

[19] Michaël Baudin, Anne Dutfoy, Bertrand Iooss, and Anne-Laure Popelin. *OpenTURNS: An Industrial Software for Uncertainty Quantification in Simulation*, pages 1–38. Springer International Publishing, Cham, 2016.

[20] Martín Abadi et al. TensorFlow: Large-scale machine learning on heterogeneous systems, 2015. Software available from tensorflow.org.